Published in final edited form as:
Adv Drug Deliv Rev. 2008 August 17; 60(11): 1241–1251. doi:10.1016/j.addr.2008.03.014.

Multifunctional magnetic nanoparticles for targeted imaging and therapy

Jason R. McCarthy† and **Ralph Weissleder**
Center for Molecular Imaging Research, Harvard Medical School and Massachusetts General Hospital, 149 13th St., Rm 5406, Charlestown, MA 02129, USA

Abstract

Magnetic nanoparticles have become important tools for the imaging of prevalent diseases, such as cancer, atherosclerosis, diabetes, and others. While first generation nanoparticles were fairly nonspecific, newer generations have been targeted to specific cell types and molecular targets via affinity ligands. Commonly, these ligands emerge from phage or small molecule screens, or are based on antibodies or aptamers. Secondary reporters and combined therapeutic molecules have further opened potential clinical applications of these materials. This review summarizes some of the recent biomedical applications of these newer magnetic nanomaterials.

Keywords

Iron oxide; magnetic nanoparticles; peptide targeting; small molecule targeting; molecular imaging; cancer; atherosclerosis; theranostic

1. Introduction

Nanotechnology plays an increasing role in molecular diagnostics, in vivo imaging, and improved treatment of disease. The usefulness of nanoparticles is mainly derived from their small size, large surface area, and kinetics for in vivo drug delivery [1].The ability to functionalize the surface with targeting ligands, as well as imaging and therapeutic moieties also allows for the creation of multimodal, multifunctional nanoagents. Metal oxides, in particular iron oxide, have been used since the early 60's for magnetic separations. In 1978, Ogushi established that magnetic nanoparticles have the ability to shorten the T2 relaxation times of water, and shortly thereafter, were used for magnetic resonance imaging [2].Over the course of the past two decades, numerous nanoparticulate iron oxide preparations have been reported, and used in cellular therapy, tissue repair, drug delivery, hyperthermia [3,4], magnetic resonance imaging (MRI) [5–7], as spoilers for magnetic resonance spectroscopy[8], for magnetic separation [9], and more recently as sensors for metabolites and other biomolecules [10–12]. Recent research has focused on the targeted delivery of iron oxide nanoparticles to sites of interest, and has been accomplished with peptides, antibodies, and small molecules. Herein, we will review the synthesis and functionalization of iron oxide nanoparticles, and explore their utility in cancer and cardiovascular applications.

Tel.: 617-726-8226, *Fax*.: 617-726-5708, *Email:* jason_mccarthy@hms.harvard.edu.

1.1. Biocompatible, coating-stabilized magnetic nanoparticles

Magnetic nanoparticles, in particular iron oxides, have been synthesized in either aqueous or organic phases. In order to impart stability and ensure nontoxicity under physiological conditions, as well as to allow for functionalization and targeting, these materials require sophisticated coatings [13]. Ideally, coating materials will have a high affinity for the iron oxide core, and be nonimmunogenic, nonantigenic, and prevent opsonization by plasma proteins. While the synthesis of particles at high temperatures in organic solvents allows for better control of particles size and morphology [14,15], the particles must be transferred to aqueous solutions for biological applications. Aqueous synthesis of iron oxide nanoparticles, on the other hand, usually involves the neutralization of acidic iron salts in the presence of a coating material [16]. Coatings have included lipids [17,18], liposomes [19,20], proteins [21,22], dendrimers [23], polyethylene glycol [24], polyacrylamide [25], polysaccharides [26,27], and bisphosphonates [28]. Most clinical preparations (Ferridex®, Combidex®, Resovist®, and AMI-228/ferumoxytrol) have been based upon dextran or similar carbohydrate coatings, partly due to their previous use as plasma expanders, and also their innate affinity for iron oxide [5–7,29–35], although one recent preparation has described the use of citrate-stabilized particles [36].

Dextran-coated iron oxide nanoparticles have become an important part of clinical cancer imaging, and have been shown to increase the accuracy of cancer nodal staging [37–39].These particles have also been utilized to better delineate primary tumors [40], image angiogenesis [41], and detect metasteses [42,43]. Additionally, these particles have been used to image the inflammatory components of atherosclerosis [44]. Modification of dextranated iron oxide with targeting ligands, such as antibodies [45], has also been accomplished, in hopes of increasing the affinity of the nanoparticles for their target tissues. One of the main drawbacks is that the dextran coating is in equilibrium with the surrounding medium, as it is not strongly associated with the iron oxide core.

One of the greatly enabling modifications made to dextran coated iron oxide nanoparticles has been the crosslinking (caging) of the dextran and its amination [16]. The resulting particle, CLIO (cross-linked iron oxide), allows for facile functionalization via amide bond formation. It also offers superb stability under harsh conditions without a change in size, blood half-life, or loss of its dextran coat. CLIO has served as an ideal model compound for many experimental applications but is unlikely to be developed for clinical use, given the epichlorohydrin-induced crosslinking, similar to Sephadex particles. In order to circumvent this, magnetic nanoparticle preparations with biodegradable, high-affinity coatings are currently in development by us and others.

1.2. Multifunctionality

The localization of nanoparticles to sites of interest is often accomplished via conjugation of targeting moieties (peptides, antibodies, aptamers, small molecules) to the particle surface. Due to the high surface area to volume ratio of nanoparticles, many copies of the ligands can be attached. This multivalent targeting makes use of the fact that multiple copies of receptors are expressed on the cell surface. If one particle is able to bind to more than one receptor, the binding affinity of the particles for the cell increases dramatically [46]. The utility of these targeted particles further increases with the addition of other ligands, such as imaging and therapeutic moieties. When the nanoparticles are functionalized with more than one type of ligand, they are termed multifunctional. A number of multifunctional nanoparticulate preparations are described in sections 4 and 5 of this review. Often, they are peptide-targeted magnetic particles bearing fluorescent dyes or radionuclides, but can also include ligands for therapy, such as near infrared light activated therapeutic agents (NILAT, section 5). Finally, multimodal nanoparticles bear complementary imaging moieties, which allow for the

investigation of the particle localization across a number of platforms, such as magnetic resonance, optical, or nuclear imaging.

2. Chemistry of surface modification

The conjugation of ligands to nanoparticles requires diverse chemistries. Below, we describe two common approaches used in the attachment of these ligands.

2.1. Conventional bioconjugation strategies

The surface of nanoparticles may be coated with a number different functionalities, depending upon the coating material and the reactive groups present on the targeting ligand. Most commonly, amines or carboxylic acids are present on the nanoparticle surface for reaction with ligands. These groups are readily interchangeable (figure 1). Reaction of amine-functionalized particles with succinic anhydride or glutaric anhydride, converts the surface to carboxylates, whereas the activation of carboxylic acid functionalized particles with 1-ethyl-3-(dimethylaminopropyl)carbodiimide (EDC) and N-hydroxysuccinimide (NHS) or N-hydroxysulfosuccinimide (sulfo-NHS) followed by reaction with a diamine results in amine-functionalized nanoparticles.

Amine-coated nanoparticles are easily modified by ligands containing NHS-modified carboxylic acids or isothiocyanates, such as fluorescein isothiocyanate (FITC). Epoxides and anhydrides can also be directly reacted in sodium bicarbonate buffer at pH 8.6 [47].In order to functionalize these particles with carboxylic acid containing ligands, the reaction must occur in the presence of activating agents such as EDC and NHS or sulfo-NHS. Ligands bearing sulfhydryl groups, such as those present in peptides, antibodies, and oligonucleotides, can also be appended to the surface of amine-coated particles once the surface is modified with heterobifunctional linkers such as succinimidyl iodoacetate (SIA), N-succinimidyl-3-(2-pyridyldithio)propionate (SPDP), or succinimidyl-4-(N-maleimidomethyl)cyclohexane-1-carboxylate (SMCC). One of the main advantages of utilizing SPDP is that it can be used to determine the number of reactive amines on the particle, as pyridine-2-thione is released upon reaction with dithiothreitol (DTT), can be detected spectrophotometrically, and thus quantitated. Reaction of ligands with SPDP functionalized particles also liberates pyridine-2-thione, thus allowing the number of conjugated species to be determined.

As opposed to amine-coated nanoparticles, which are readily conjugated to a number of reactive ligands, carboxylic acid-coated particles require activation prior to conjugation. Amine containing ligands are typically conjugated to carboxylic acid functionalized particles in the presence of EDC and sulfo-NHS to yield the corresponding amide. Although fairly tedious, the reaction of ligands containing hydroxyl groups is also accomplished with the carboxylic acid coated particles. Initially, the particles must be precipitated from aqueous solution by addition of acetone, and are then washed thrice with acetone to remove the residual water. The particles are then suspended in anhydrous dimethylsulfoxide (DMSO) and thionyl chloride is added in order to form the corresponding acid chloride. Once the activation has been accomplished, a drop of water is added to the solution to quench the remaining thionyl chloride, followed by addition of an excess of the alcohol and a base catalyst. In all instances the purification of the functionalized particles is facilitated by gel filtration.

2.2. Click chemistry

The Huisgen 1,3-dipolar cycloaddition, also known as the “click reaction,” is also highly useful in the functionalization of iron oxide nanoparticles. These reactions have several advantages over the above bioconjugations. First, click reaction can occur under relatively mild conditions in aqueous solutions. These reactions are also highly specific, occur with high yields, and do

not produce undesirable side products, such as dicyclohexylurea, which is resultant from the use of the activating agent dicyclohexyl-carbodimide (DCC)[48]. Lastly, triazoles are biocompatible entities, and are seen in several Food and Drug Administration (FDA) approved drugs, including Triazolam, which is used to treat insomnia. The Cu(I) catalyzed reaction between alkyne and azide groups results in the formation of a stable triazole linkage. The robustness of this technique has been demonstrated with CLIO [49]. CLIO can be functionalized with azide or alkyne moieties by reaction of carboxylic acid-functionalized particles with azido propylamine or propargylamine in the presence of activating reagents, such as EDC and sulfo-NHS in 2-(N-morpholino)ethanesulfonic acid (MES) buffer at pH 6.0. As proof-of-principle, several biologically relevant molecules were modified to contain the corresponding azide or alkyne moiety. The succinimidyl esters of biotin or VivoTag-S 680 (a near infrared fluorophore), or the isothiocyanate of fluorescein, were directly reacted with azido propylamine or propargylamine, while ligands containing hydroxyl groups, such as estradiol, paclitaxel, and Disperse Red 1, were first activated with 1,1'-carbonyldiimidazole (CDI), followed by reaction with the alkynyl or azido amine. Conjugation reactions between the functionalized nanoparticles and ligands occurred in aqueous solution at 37 °C for 5–8 hours, resulting in greater than 90% conversion.

3. Targeting of iron oxide nanoparticles

Table 1 summarizes a number of different ligands and approaches that have recently been investigated for in vivo targeting of magnetic nanoparticles.

3.1. Peptides as affinity ligands

The identification of peptide ligands has been accomplished mainly via phage screening and *in silico* data mining of available electronic resources or databases. Phage display is a technique which involves the synthesis of libraries of heterogenous bacteriophage, viruses that infect bacterial cells, by standard recombinant DNA technology, each expressing a different peptide sequence on its coat. Plate-based phage screens have historically been performed against immobilized proteins. This technique is advantageous, as the binding partner of the peptide sequence is already known. After the bound phage is identified, it is expanded and sequenced to determine the targeting peptide sequence. Unfortunately, the target may not be in its native state, which may cause the efficacy of the peptide to be decreased in in vivo applications. In order to circumvent this, cell-based phage screens have been developed.The main advantage of these systems is that they allow for the targeting of specific cell types with no *a priori* knowledge, although specific biomarkers can also be screened for. Cell-based screens can also be biased towards phage that have been internalized. Peptide sequences identified through this method are useful in the development of imaging agents, as the agents derived from them are also internalized by cells, leading to amplification of the signal through accumulation. One further modification of cell-based phage display is the potential to screen libraries under modified non-static in vitro conditions, such as flow. This results in phage that are able to bind more efficaciously in vivo, especially to targets that are expressed in the vasculature, where sheer stress will cause the dissociation of weakly bound peptides from their targets. Finally, and most importantly for targeting, in vivo phage screening is increasingly being used. Injection of phage libraries into model animals followed by harvesting of the desired tissues can identify phage that are able to traverse the numerous barriers presented in vivo. Recently, phage have also been explored for direct screening of targets by functionalization with fluorophores or magnetic nanoparticles.[77] The apparent efficacy of these peptide sequences are presented below in a number of pertinent examples of targeted imaging and theranostic agents.

Efficacious peptide targeting ligands can also been identified by searches of electronic resources. While many databases have existed for protein sequences and interactions, analogous resources for peptides are scarce. In order to facilitate expeditious identification of

potential targeting peptides, a novel, searchable database, PepBank, has recently been created by us (http://pepbank.mgh.harvard.edu/). The database currently contains over 20000 peptide sequences and enjoys a number of simple or advanced search capabilities. This database has identified prospective peptide sequences by text mining of Medline abstracts, full text PDF files, and other databases, such as ASPD and Uniprot. One of the main advantages of the database is that a search for a specific sequence may result in a number of similarities to known peptides, while one detractor is that the researcher is limited to the sequences that have already been identified and contained within the database.

3.2. Small molecules as targeting ligands

The modification of the surface of nanoparticles with small molecules as targeting ligands has recently been described as an alternative targeting strategy, with potential for major biomedical advances. This is due to the ability to functionalize the particle surface with an increased number ligands with limited steric constraints, due to their small size versus peptides and antibodies. The ability to load more targeting ligands also increases possible multivalent effects between the particle and its target. The ability to synthesize large numbers of functionally diverse molecules has been facilitated by advances in diversity-oriented synthesis (DOS). This has yielded numerous libraries of complex, natural product-like molecules. In tandem with advances in high-throughput screening and approaches to rapidly functionalize particle surfaces, preliminary studies have been undertaken to investigate the ability of small molecules to effect the in vitro and in vivo uptake of nanoparticles.

We have previously synthesized a library of 146 differently functionalized particles, utilizing FITC-labeled CLIO as a model magnetofluorescent reporter [68]. Small, water soluble molecules, with molecular weights less than 500 Da and containing reactive amines, alcohols, carboxylic acids, sulfhydryls or anhydrides were used, excluding those compounds that are known to bind to proteins, resulting in nanoparticles decorated with up to 60 targeting moieties. The particles were then screened against a number of cell lines (e.g. human umbilical vein endothelial cells (HUVEC), resting primary human macrophages, granulocyte macrophage colony stimulating factor-stimulated primary macrophages, a human macrophage-like cell line (U937), and human pancreatic ductal adenocarcinoma cells (PaCa-2) to determine whether the modifications change the affinity of the particles versus the unmodified amino-CLIO (figure 2) One of the main tasks was to determine if the particles could differentiate between closely related functional states of cells, such as resting and activated macrophages.

Following incubation with the respective particle formulation and washing, the uptake of each particle was assayed by fluorescence microscopy, flow cytometry, or an immunoassay for FITC. In general, the amount of cellular uptake was greatly varied (2 – 2,239 fg Fe/cell) within each cell type and across the different cell types. In particular, two preparations (CLIO-gly and CLIO-bentri) stood out due to their differing uptake into macrophage subtypes. These particles were scaled up and tested in a series of activated macrophages. Modification of CLIO with glycine resulted in nanoparticles which were taken up readily by activate macrophages but not by resting macrophages. Conversely, bentri-modified particles demonstrated little uptake by activated macrophages, while demonstrating a high avidity for resting macrophages. The authors reasoned that these materials may find use in targeting diseases with inflammatory components, such as atherosclerosis.

4. Examples of multimodal imaging

The following examples of targeted delivery of imaging agents summarize some of the most recent approaches undertaken by us and others. These examples serve to illustrate the number of new targets and conjugation strategies that have been utilized.For a more comprehensive list, see table 1.

4.1. Molecular imaging in atherosclerosis

4.1.1. Macrophage avid iron oxide nanoparticles—Macrophages are a key component of atherosclerotic vessels and can constitute up to 10–20% of the cells present within culprit lesions. In particular, macrophages contribute crucially to all stages of atherogenesis, and are involved in plaque rupture leading to fatal thrombosis in advanced lesions [78–80]. Due to the morbidity and mortality associated with atherosclerotic vascular disease, novel methods to identify and treat inflamed atheromata are needed.

One of the approaches taken to identify suspect lesions has been the use of magnetic nanoparticles to image macrophages. Clinically, this has been illustrated in our own trials in the early 90's and more recently in human carotid atheroma by Trivedi *et al.* using dextran-coated iron oxide nanoparticles [44,81]. When the authors injected the nanoparticle preparation into symptomatic patients with severe internal carotid artery stenosis, areas of signal loss corresponding to the lesions became evident 24–48 hours post-injection, which was further corroborated by histology.

The imaging capabilities of these nanomaterials were further extended with the addition of fluorophores to the particles, allowing for the use of a multitude of optical imaging modalities alongside the commonly used MR imaging. Jaffer and co-workers have utilized fluorophore-derived CLIO to investigate its localization within atherosclerotic lesions, and were able to visualize inflamed plaques both by MR and optical imaging modalities [82,83]. Recently, the cellular localization of CLIO labeled with both a fluorophore and radionuclide (^{64}Cu) within these lesions was also investigated (figure 3)[84] Following injection of the nanoparticle preparation and sacrifice of the animals, the aortas were excised, digested, and characterized by flow cytometry. Data analysis revealed that about 75% of the nanoparticles within the atherosclerotic lesions were associated with macrophages, 20% with neutrophils, and the remainder with endothelial cells, lymphocytes and smooth muscle cells.

4.1.2. Vascular cell adhesion molecule-1—Vascular cell adhesion molecule-1 (VCAM-1) is expressed on activated endothelial cells, macrophages, and smooth muscle cells, and participates in the initiation of the inflammatory process, as well as the progression of atherosclerotic lesions. Thus, it serves as a potentially useful imaging target. In one approach, antibodies have been conjugated to magnetofluorescent nanoparticles [53]. Conjugation of anti-VCAM-1 or IgG (control) antibodies was accomplished by activation of carboxylic acid functionalized CLIO with EDC/NHS followed by reaction with the respective antibody to yield 0.87 mg anti-VCAM-1 (~ 3 per particle) and 0.63 mg IgG (~ 2 per particle) per mg of iron. Once synthesized, the preferential targeting ability of the particles were tested in vitro against primary cultures of murine heart endothelial cells (MHEC) expressing high levels of VCAM-1, and murine dermal endothelial cells (MDMEC) with low VCAM-1 expression. Flow cytometry demonstrated binding of the VCAM-1 targeted particle to the MCEC cells, whereas there was no binding to the MDMEC cells. The in vivo targeting ability of the conjugate was next tested in a murine model of inflammation. In this model, one ear of the mouse in injected with tumor necrosis factor- (TNF-), which induces a severe local inflammatory response. The opposite ear remains inflammation free and serves as the control. After injection, the VCAM-1 targeted particles demonstrated binding on the surface of the vasculature in the TNF- treated ear, with peak labeling 6 hours post-injection, as determined by intravital fluorescence microscopy (IVFM). Whereas 24 hours after injection, the signal had grown faint, possibly due to the dissociation of the particles from the endothelium. A similar VCAM-1 antibody-based targeting strategy was recently repeated by Choudhury and co-workers using micron sized iron oxide particles to image inflammation in the brain [85].

Due to the drawbacks experienced in the use of antibody-modified nanoparticles, such as lack of cellular internalization and limited loading of the surface of the nanoparticle, peptide based

targeting moieties have been investigated. Using phage display, Kelly *et al.* have identified two potentially useful peptide sequences by phage display targeting VCAM-1. The first peptide was derived from cyclic peptide phage libraries screened against murine cardiac endothelial cells (MCEC) that express high levels of VCAM-1, and was identified as CVHSPNKKC (VHS) [54]. In order to impart upon the peptide sequence conjugatable functionalities, a C-terminal GGSKGC sequence was appended. When fluorescently labeled, the peptide exhibits rapid internalization by MCECs, versus a scrambled control peptide. When the cells are pre-incubated with an anti-VCAM-1 antibody, actively blocking the VCAM-1 binding sited, neither the VHS or control peptides are internalized by the cells. When conjugated to magnetofluorescent nanoparticles modified with Cy 5.5, the peptide targeted particles exhibited a 10-fold increase in uptake versus the control particle.

The in vivo targeting ability of the peptide was tested in the TNF- inflammation model. Four hours after injection of the VHS peptide targeted nanoparticle or the control, only the targeted agent remained bound to the inflamed vasculature, as observed by intravital fluorescence microscopy (IVFM). In the control ear, very little accumulation of the particles was observed. Interestingly, at 24 hours post-injection of the nanoagent, significant signal from the targeted particles was still observed in the inflamed ear. These observations were further corroborated histologically. The VCAM-1 targeted nanoagents also demonstrated utility in its ability to localize atherosclerotic lesions by MRI in apolipoprotein E knockout mice (apoE$^{-/-}$), which spontaneously develop atheromata, especially when fed a high fat diet. Following intravenous injection of the VHS nanoparticle, significant signal decrease was observed in the aortic wall. This result was not observed in mice injected with an untargeted control nanoparticle, or in C57BL/6 wild type mice without atherosclerotic lesions.

More recently, Kelly and coworkers have identified a second, linear peptide sequence that targets VCAM-1 by both in vitro and in vivo phage display [55,56]. The resulting peptide, VHPKQHR (termed termed VCAM-1 internalizing peptide, VINP, by the authors), demonstrated a 20-fold increase in binding to MCECs, as compared to the VHS peptide. When conjugated to a Cy 5.5-labeled nanoparticle, the agent demonstrated excellent uptake in both the TNF- inflammation model, and in atherosclerotic apoE$^{-/-}$ mice, as the VHS-modified particles had previously (figure 4). Interestingly, the authors tested the nanoagent against freshly resected human endarterectomy specimens. The samples were incubated with either saline or the VINP-labeled nanoparticles for 24 hours, and were investigated with both MRI and fluorescence imaging. As compared to the control samples, the VINP-particles demonstrated a marked decrease in T2 signal, as is expected for iron oxide nanoparticles, whereas fluorescence reflectance imaging revealed a strong fluorescence enhancement from the targeted particles.

4.2. Molecular imaging in cancer

4.2.1. Hepsin-targeted detection of prostate cancer—In one recent example, Kelly *et al.* have demonstrate the utility of imaging hepsin expression in prostate cancer [69]. Hepsin is a type II transmembrane serine protease that is expressed in precursor lesions, high-grade prostate intra-epithelial neoplasia, and in hormone-refractory metastatic tumors [86]. To date, there are no commercially available HPN ligands that are not antibody-based. Thus, phage screening against PC3 cells stably transfected to overexpress HPN (HPN-PC3) was able to identify a consensus binding sequence, IPLVVPL. The resultant targeting peptide, bearing a GGSKGC C-terminal sequence in order to label it with fluorescein and to enable it to be conjugated to a nanoparticle was tested against HPN-PC3 and LNCaP cells which express HPN, and PC3 and DU145 cells which no not express HPN. The peptide was found to bind avidly to both of the HPN-expressing cell lines, whereas the binding to the other cell lines was

minimal. Hepsin binding of the peptide was further confirmed by preincubation of HPN-PC3 cells an anti-hepsin antibody, as it abrogated binding of the peptide by 84.4%.

Conjugation of the peptide to CLIO was accomplished by reaction of amine functionalized CLIO with SIA, followed by reaction with the fluorescein labeled peptide. As compared to the free peptide, the nanoparticle demonstrated 10-fold greater cell-associated fluorescence, possibly due to the multivalency of the particle (figure 5). The targeted particle also bound to the PC3 cells 80-fold less than the HPN-PC3 cells. The in vivo utility was tested in mouse xenographs of prostate tumors. demonstrating significantly higher accumulation in the LNCaP tumors than in the PC3 tumors (65 ± 3.1 nM vs 23 ± 1.6 nM particle).

4.2.2. Homing to tumor vasculature—A number of endothelial targets have been explored to image tumor neovasculature. In one example, Ruoslahti and coworkers have utilized in vivo phage screens of tumor-bearing transgenic breast cancer mice to discover a peptide sequence, CREKA, that homes to this target [70]. When fluorescently labeled and intravenously injected into transgenic- or xenograph tumor bearing mice, the peptide readily accumulates within the tumors, whereas it is undetectable in normal tissues. Interestingly, the peptide formed a “distinct meshwork in the tumor stroma,” which led the authors to hypothesize that the peptide was binding to clotted plasma proteins within the tumor. In order to test this, the peptide was injected into tumor-bearing fibrinogen knockout mice, which lack tumoral fibrin, and did not demonstrate accumulation, verifying that CREKA homes to clots.

The FITC-labeled peptide was next conjugated to CLIO through the N-terminal cysteine after modification of the particle with the heterobifunctional linker N-[a-maleimidoacetoxy] succinimide ester (AMAS), resulting in approximately 8000 peptides per particle. The CREKA-modified particles demonstrated binding to both human and mouse plasma clots in vivo, which could be inhibited by preincubation with the free peptide. Initial in vivo tests of the homing ability of the particles to MDA-MB-435 breast cancer xenographs showed poor uptake in the tumors, whereas the majority of the agent localized to the reticuloendothelial system (RES), presumably through protein opsonization. In order to circumvent this, decoy liposomes decorated with Ni(II) chelates were injected to deplete plasma opsonins and allow for targeted delivery of the nanoparticle. Following liposome treatment, large amounts of the targeted particles were observed in the tumor vasculature, with up to 20% of the vessels filled with fluorescent masses. IVFM was also undertaken with Dil-labeled erythrocytes to monitor the time course of clot formation. As the clot formed, blood flow obstruction became evident concomitant with CREKA-labeled particle entrapment. In order to test the amplification of tumor targeting due to clot formation, mice were pretreated with heparin prior to injection of the particles. Although clots were not formed, binding of the particles to the walls of the vessels was still observed, possibly due to fibrin already present in the tumor vasculature. This also demonstrated that the CREKA peptide induces clot formation, which, in turn binds more particles, causing amplification of the targeting. In one last experiment, the CREKA-particles were labeled with Cy 7, were injected into tumor bearing mice, and were imaged by fluorescence reflectance imaging (FRI, figure 6). In particle treated mice, the tumor was clearly delineated, while those mice treated with the targeted particle and heparin showed a reduced signal from the tumor.

Homing to tumor vasculature has also been accomplished by Montet *et al.* using a fluorescently labeled CLIO bearing RGD peptides [46,62]. The tripeptide sequence RGD targets **V 3 integrin, which is upregulated in angiogenic endothelial cells.** In vitro, the particles demonstrated 40-fold higher binding to **V 3 expressing BT**-20 human breast carcinoma cells than a control particle, and 5-fold higher binding to BT-20 cells than to 9L rat gliosarcoma cells, which express low levels of **V 3. In vivo, the targeted** particles demonstrated 6.5-fold higher uptake in BT-20 tumors than the control particle and 1.8-fold higher uptake in 9L tumors,

as determined by FMT. Homing of the particles to the tumor vasculature was further confirmed histologically.

5. Theranostic Nanoagents

The ability of nanoparticles to both diagnose and treat diseases is an emerging concept. These nanoagents have been termed theranostic due to their diagnostic and therapeutic capabilities.

5.1 Near infrared light activated therapeutics

It has been hypothesized that selective “silencing” of activated macrophages in atherosclerotic lesions (as opposed to all macrophages or resting macrophages) can lead to long lasting therapeutic effects, including the stabilization of inflamed, vulnerable atheromata. Macrophages play a critical role in atherosclerosis, as they secrete proteolytic enzymes which cause degradation of fibrous caps, promote atherothrombosis, and/or play other key roles in the progressive inflammatory cascade. We have recently reported on the conjugation of porphyrinic photosensitizers to macrophage avid magnetofluorescent nanoparticles [87]. These particles make use of the fact that wavelengths in near infrared region of the electromagnetic spectrum are able to penetrate deeper into tissues, and are thus useful in near infrared fluorescence (NIRF) imaging, and thus, also near infrared light activated therapy (NILAT). To this end, a CLIO-based theranostic nanoparticle incorporating a potent NILAT agent, as well as Alexa Fluor 750 (AF750) for use in optical imaging has been developed. Both components are conjugated to amine functionalized CLIO via reaction with the respective succinimide ester in a ratio of 10 NILAT moieties and 3 AF750 per particle. The excitation wavelengths of the diagnostic and therapeutic portions are spectrally distinct, allowing for the localization of the particle to be determined without causing extraneous cell killing.

Cell based assays of the uptake and phototoxicity of the theranostic nanoagent were accomplished in murine macrophages (RAW 246.7). The particles demonstrated time-dependent uptake, as determined by flow cytometry. At saturation, each macro-phage was calculated to contain between 10^6 and 10^7 particles per cell. Phototoxicity was assayed by a cell proliferation assay (MTS). In the absence of light, the agent did not display any more toxicity than control particles without the NILAT agent. However, when the cells were irradiated at 650 nm (the therapeutic wavelength) a dose-dependent phototoxicity was observed. More importantly, when the cells were irradiated at 750 nm with a light dose comparable to that used in IVFM, minimal cell death was observed. In another experiment, the nanoagent was incubated with transformed human macrophages (U937), and brought about 100% cell death after 1 hour incubation and laser illumination. Ongoing in vivo experiments have demonstrated that the nanoagent preferentially accumulates within atherosclerotic lesions within 24 hours of intravenous injection, as determined by IVFM. Irradiation of atheroma at the therapeutic wavelength (650 nm) results in macrophage cell death within 24 hours of therapy. At 1 week post therapy, reinjection of the therapeutic nanoagent results in minimal uptake by the lesion, intimating a significant reduction in macrophage content, while histology of the plaque at 3 weeks demonstrates a thickened fibrous cap and decreased inflammation. Further experiments to demonstrate therapeutic efficacy and plaque stabilization are in progress.

A team led by Brian Ross has also synthesized a light-activated theranostic nanoagent for the imaging and treatment or brain tumors, based upon the encapsulation of iron oxide nanoparticles and the photosensitizer Photofrin within PEGylated amine functionalized polyacrylamide nanoparticles [71]. These particles were targeted using a vascular homing peptide, F3, identified by phage screens, which is a 31-amino acid sequence present at the N-terminus of human high-mobility group protein 2. F3 binds to nucleolin on the surface of tumor cells and angiogenic endothelial cells, which subsequently traffics it to the nucleus. In order

to determine cellular uptake and subcellular localization, the particles were also fluorescently labeled with Alexa Fluor 594. The resulting particles were approximately 40 nm in diameter, and were appended with 30 peptides and 10 fluorophores.

Cellular uptake and phototoxicity of the particles was determined after 4 hours incubation with the targeted particles. Fluorescence microscopy revealed significant uptake and cell surface binding of the F3-labeled particles to MDA-MB-435 breast cancer cells, which readily translated to potent phototoxicity, with over 90% of the cells receiving the targeted particles dying.

The in vivo efficacy of the nanoparticles was investigated in rat brain tumor model. Glioma cells (9L) were implanted in the right forebrain of the animals, and were allowed to grow for 12 days prior to administration of the theranostic agent. The localization of the nanoparticles was determined by serial MR imaging after injection of the targeted and untargeted preparations. Within 10 minutes, the both particles demonstrated significant enhancement of the tumor. Over the course the next 2 hours, the nontargeted particles washed out of the tumor, whereas the F3-targeted agent continued to accumulate. According to analysis of the dynamic scanning MRI data, F3-modification of the polyacrylamide nanoparticles increases the tumor half-life from 39 to 123 minutes.

The therapeutic efficacy of nanoparticles was subsequently evaluated in comparison to the unencapsulated photosensitizer, and was determined by changes in tumoral diffusion, as measured by MRI (figure 7). While rats treated with Photofrin or untargeted particles demonstrated similar changes in diffusion 8 days post-therapy (~ 25%), the diffusion values of the rats receiving the F3-targeted particles increased more significantly (~ 40%) versus controls (~ 10%). In fact, the animals that demonstrated the largest increase in diffusion values were also the ones who survived the longest. Whereas the median survival time for the Photofrin and untargeted particle groups were 13 days (versus 7 days for the control group), the animals treated with the targeted agent had a median survival of 33 days, with 2 animals disease-free 6 months after therapy.

6. Future perspectives

While iron oxide nanoparticles have found clinical utility in the magnetic resonance imaging of numerous diseases, targeted delivery of these agents in the clinical setting using antibodies, peptides, or small molecules has yet to come to fruition. The generation of multifunctional nanoparticles will allow for the investigation of diseases across a number of imaging platforms, and enable the accumulation of vast amount of information relevant to patient care. The ultimate goal in the synthesis of multifunctional nanoparticles is the creation of theranostic nanoagents, thus enabling the targeted diagnosis and treatment of disease.

Acknowledgements

This work was supported by NIH grants U01-HL080731 (RW), U54-CA119349 (RW), and U54-CA126515 (RW). We thank all CMIR lab members for many helpful discussions, in particular, Drs. Josephson, Kelly and Nahrendorf.

References

1. Maeda H, Wu J, Sawa T, Matsumura Y, Hori K. Tumor vascular permeability and the EPR effect in macromolecular therapeutics: A review. J Control Release 65;2000:271–284.
2. Ohgushi M, Nagayama K, Wada A. Dextran-magnetite: A new relaxation reagent and its application to T2 measurements in gel systems. Journal of Magnetic Resonance (1969–1992) 1978;29:599–601.
3. Halbreich A, Roger J, Pons JN, Geldwerth D, Da Silva MF, Roudier M, Bacri JC. Biomedical applications of maghemite ferrofluid. Biochimie 1998;80:379–390. [PubMed: 9782379]

4. Pankhurst QA, Connolly J, Jones SK, Dobson J. Applications of magnetic nanopartiocles in biomedicine. J Phys D: Appl Phys 2003;36:R167–R181.
5. Weissleder R, Stark DD, Compton CC, Wittenberg J, Ferrucci JT. Ferrite-enhanced MR imaging of hepatic lymphoma: An experimental study in rats. AJR Am J Roentgenol 1987;149:1161–1165. [PubMed: 3318339]
6. Weissleder R, Hahn PF, Stark DD, Rummeny E, Saini S, Wittenberg J, Ferrucci JT. MR imaging of splenic metastases: Ferrite-enhanced detection in rats. AJR Am J Roentgenol 1987;149:723–726. [PubMed: 3498320]
7. Weissleder R, Elizondo G, Wittenberg J, Lee AS, Josephson L, Brady TJ. Ultrasmall superparamagnetic iron oxide: An intravenous contrast agent for assessing lymph nodes with MR imaging. Radiology 1990;175(2):494–498. [PubMed: 2326475]
8. Le Duc G, Vander Elst L, Colet JM, Roch A, Gillis P, Le Bas JF, Muller RN. Ultrasmall particulate iron oxides as contrast agents for magnetic resonance spectroscopy: A dose-effect study. J Magn Reson Imaging 2001;13:619–626. [PubMed: 11276108]
9. Whitesides GM, Kazlauskas RJ, Josephson L. Magnetic separations in biotechnology. Trends in Biotechnology 1983;1:144–148.
10. Grimm J, Perez JM, Josephson L, Weissleder R. Novel nanosensors for rapid analysis of telomerase activity. Cancer Res 2004;64:639–643. [PubMed: 14744779]
11. Kim GY, Josephson L, Langer R, Cima MJ. Magnetic relaxation switch detection of human chorionic gonadotrophin. Bioconjug Chem. 2007
12. Perez JM, Josephson L, O'Loughlin T, Hogemann D, Weissleder R. Magnetic relaxation switches capable of sensing molecular interactions. Nat Biotechnol 2002;20:816–820. [PubMed: 12134166]
13. Qin J, Laurent S, Jo YS, Roch A, Mikhaylova M, Bhujwalla ZM, Muller RN, Muhammed M. A high-performance magnetic resonance imaging T2 contrast agent. Advanced Materials 2007;19:1874–1878.
14. Hou Y, Xu Z, Sun S. Controlled synthesis and chemical conversions of FeO nanoparticles. Angew Chem Int Ed Engl 2007;46:6329–6332. [PubMed: 17645273]
15. Rockenberger J, Scher EC, Alivisatos AP. A new nonhydrolytic single-precursor approach to surfactant-capped nanocrystals of transition metal oxides. J. Am.Chem. Soc 1999;121:11595–11596.
16. Josephson L, Tung CH, Moore A, Weissleder R. High-efficiency intracellular magnetic labeling with novel superparamagnetic-tat peptide conjugates. Bioconjug Chem 1999;10:186–191. [PubMed: 10077466]
17. De Cuyper M, Joniau M. Mechanistic aspects of the adsorption of phospholipids onto lauric acid stabilized magnetite nanocolloids. Langmuir 1991;7:647–652.
18. Nitin N, LaConte LE, Zurkiya O, Hu X, Bao G. Functionalization and peptide-based delivery of magnetic nanoparticles as an intracellular MRI contrast agent. J Biol Inorg Chem 2004;9:706–712. [PubMed: 15232722]
19. Bogdanov AA, Martin C, Weissleder R, Brady TJ. Trapping of dextran-coated colloids in liposomes by transient binding to aminophospholipid: preparation of ferrosomes. Biochim Biophys Acta 1994;1193:212–218. [PubMed: 7518693]
20. Bulte JW, De Cuyper M. Magnetoliposomes as contrast agents. Methods Enzymol 2003;373:175–198. [PubMed: 14714404]
21. Bulte JW, Douglas T, Mann S, Frankel RB, Moskowitz BM, Brooks RA, Baumgarner CD, Vymazal J, Strub MP, Frank JA. Magnetoferritin: Characterization of a novel superparamagnetic MR contrast agent. J Magn Reson Imaging 1994;4:497–505. [PubMed: 7802866]
22. Wilhelm C, Billotey C, Roger J, Pons JN, Bacri JC, Gazeau F. Intracellular uptake of anionic superparamagnetic nanoparticles as a function of their surface coating. Biomaterials 2003;24:1001–1011. [PubMed: 12504522]
23. Bulte JW, Douglas T, Witwer B, Zhang SC, Strable E, Lewis BK, Zywicke H, Miller B, van Gelderen P, Moskowitz BM, Duncan ID, Frank JA. Magnetoden-drimers allow endosomal magnetic labeling and in vivo tracking of stem cells. Nat Biotechnol 2001;19:1141–1147. [PubMed: 11731783]
24. Illum L, Church AE, Butterworth MD, Arien A, Whetstone J, Davis SS. Development of systems for targeting the regional lymph nodes for diagnostic imaging: In vivo behaviour of colloidal peg-coated

magnetite nanospheres in the rat following interstitial administration. Pharm Res 2001;18:640–645. [PubMed: 11465419]

25. Moffat BA, Reddy GR, McConville P, Hall DE, Chenevert TL, Kopelman RR, Philbert M, Weissleder R, Rehemtulla A, Ross BD. A novel polyacrylamide magnetic nanoparticle contrast agent for molecular imaging using MRI. Mol Imaging 2003;2:324–332. [PubMed: 14717331]
26. Kellar KE, Fujii DK, Gunther WH, Briley-Saebo K, Bjornerud A, Spiller M, Koenig SH. Nc100150 injection, a preparation of optimized iron oxide nanoparticles for positive-contrast MR angiography. J Magn Reson Imaging 2000;11:488–494. [PubMed: 10813858]
27. Kellar KE, Fujii DK, Gunther WH, Briley-Saebo K, Spiller M, Koenig SH. 'Nc100150', a preparation of iron oxide nanoparticles ideal for positive-contrast MR angiography. Magma 1999;8:207–213. [PubMed: 10504049]
28. Portet D, Denizot B, Rump E, Lejeune JJ, Jallet P. Nonpolymeric coatings of iron oxide colloids for biological use as magnetic resonance imaging contrast agents. J Colloid Interface Sci 2001;238:37–42. [PubMed: 11350133]
29. Stark DD, Weissleder R, Elizondo G, Hahn PF, Saini S, Todd LE, Wittenberg J, Ferrucci JT. Superparamagnetic iron oxide: Clinical application as a contrast agent for MR imaging of the liver. Radiology 1988;168:297–301. [PubMed: 3393649]
30. Weissleder R, Elizondo G, Stark DD, Hahn PF, Marfil J, Gonzalez JF, Saini S, Todd LE, Ferrucci JT. The diagnosis of splenic lymphoma by MR imaging: Value of superparamagnetic iron oxide. AJR Am J Roentgenol 1989;152:175–180. [PubMed: 2783273]
31. Weissleder R, Stark DD. Magnetic resonance imaging of the liver. Magn Reson Q 5 1989:97–121.
32. Weissleder R, Stark DD. Magnetic resonance imaging of liver tumors. Semin Ultrasound CT MR 10 1989:63–77.
33. Weissleder R, Stark DD, Engelstad BL, Bacon BR, Compton CC, White DL, Jacobs P, Lewis J. Superparamagnetic iron oxide: Pharmacokinetics and toxicity. Am J Roentgenol 1989;152:167–173. [PubMed: 2783272]
34. Weissleder R, Elizondo G, Wittenberg J, Rabito CA, Bengele HH, Josephson L. Ultrasmall superparamagnetic iron oxide: Characterization of a new class of contrast agents for MR imaging. Radiology 1990;175:489–493. [PubMed: 2326474]
35. Jung CW. Surface properties of superparamagnetic iron oxide MR contrast agents: Ferumoxides, ferumoxtran, ferumoxsil. Magn Reson Imaging 1995;13:675–691. [PubMed: 8569442]
36. Taupitz M, Wagner S, Schnorr J, Kravec I, Pilgrimm H, Bergmann-Fritsch H, Hamm B. Phase I clinical evaluation of citrate-coated monocrystalline very small superparamagnetic iron oxide particles as a new contrast medium for magnetic resonance imaging. Invest Radiol 2004;39:394–405. [PubMed: 15194910]
37. Ferrari M. Cancer nanotechnology: Opportunities and challenges. Nat Rev Cancer 2005;5:161–171. [PubMed: 15738981]
38. Harisinghani MG, Barentsz J, Hahn PF, Deserno WM, Tabatabaei S, van de Kaa CH, de la Rosette J, Weissleder R. Noninvasive detection of clinically occult lymph-node metastases in prostate cancer. N Engl J Med 2003;348:2491–2499. [PubMed: 12815134]
39. Harisinghani MG, Weissleder R. Sensitive, noninvasive detection of lymph node metastases. PLoS Med 2004;1:e66. [PubMed: 15630471]
40. Enochs WS, Harsh G, Hochberg F, Weissleder R. Improved delineation of human brain tumors on mr images using a long-circulating, superparamagnetic iron oxide agent. J Magn Reson Imaging 1999;9:228–232. [PubMed: 10077018]
41. Tang Y, Kim M, Carrasco D, Kung AL, Chin L, Weissleder R. In vivo assessment of ras-dependent maintenance of tumor angiogenesis by real-time magnetic resonance imaging. Cancer Res 2005;65:8324–8330. [PubMed: 16166309]
42. Harisinghani MG, Saini S, Weissleder R, Rubin D, deLange E, Harms S, Weinreb J, Small W, Sukerkar A, Brown JJ, Zelch J, Lucas M, Morris M, Hahn PF. Splenic imaging with ultrasmall superparamagnetic iron oxide ferumoxtran-10 (ami-7227): Preliminary observations. J Comput Assist Tomogr 2001;25:770–776. [PubMed: 11584239]

43. Saini S, Sharma R, Baron RL, Turner DA, Ros PR, Hahn PF, Small WC, Delange EE, Stillman AE, Edelman RR, Runge VM, Outwater EK. Multicentre dose-ranging study on the efficacy of USPIO ferumoxtran-10 for liver MR imaging. Clin Radiol 2000;55:690–695. [PubMed: 10988047]
44. Trivedi RA, JM UK-I, Graves MJ, Kirkpatrick PJ, Gillard JH. Noninvasive imaging of carotid plaque inflammation. Neurology 2004;63:187–188. [PubMed: 15249641]
45. Weissleder R, Lee AS, Khaw BA, Shen T, Brady TJ. Antimyosin-labeled monocrystalline iron oxide allows detection of myocardial infarct: MR antibody imaging. Radiology 1992;182:381–385. [PubMed: 1732953]
46. Montet X, Funovics M, Montet-Abou K, Weissleder R, Josephson L. Multivalent effects of RGD peptides obtained by nanoparticle display. J Med Chem 2006;49:6087–6093. [PubMed: 17004722]
47. Sun EY, Josephson L, Kelly KA, Weissleder R. Development of nanoparticle libraries for biosensing. Bioconjug Chem 2006;17:109–113. [PubMed: 16417258]
48. Devaraj NK, Collman JP. Copper catalyzed azide-alkyne cycloadditions on solid surfaces: Applications and future directions. QSAR & Combinatorial Science. 2007In Press
49. Sun EY, Josephson L, Weissleder R. "Clickable" nanoparticles for targeted imaging. Mol Imaging 2006;5:122–128. [PubMed: 16954026]
50. Hogemann D, Josephson L, Weissleder R, Basilion JP. Improvement of MRI probes to allow efficient detection of gene expression. Bioconjug Chem 2000;11:941–946. [PubMed: 11087345]
51. Weissleder R, Moore A, Mahmood U, Bhorade R, Benveniste H, Chiocca EA, Basilion JP. In vivo magnetic resonance imaging of transgene expression. Nat Med 2000;6:351–355. [PubMed: 10700241]
52. Moore A, Josephson L, Bhorade RM, Basilion JP, Weissleder R. Human transferring receptor gene as a marker gene for mr imaging. Radiology 2001;221:244–250. [PubMed: 11568347]
53. Tsourkas A, Shinde-Patil VR, Kelly KA, Patel P, Wolley A, Allport JR, Weissleder R. In vivo imaging of activated endothelium using an anti-vcam-1 magnetooptical probe. Bioconjug Chem 2005;16:576–581. [PubMed: 15898724]
54. Kelly KA, Allport JR, Tsourkas A, Shinde-Patil VR, Josephson L, Weissleder R. Detection of vascular adhesion molecule-1 expression using a novel multimodal nanoparticle. Circ Res 2005;96:327–336. [PubMed: 15653572]
55. Kelly KA, Nahrendorf M, Yu AM, Reynolds F, Weissleder R. In vivo phage display selection yields atherosclerotic plaque targeted peptides for imaging. Mol Imaging Biol 2006;8:201–207. [PubMed: 16791746]
56. Nahrendorf M, Jaffer FA, Kelly KA, Sosnovik DE, Aikawa E, Libby P, Weissleder R. Noninvasive vascular cell adhesion molecule-1 imaging identifies inflammatory activation of cells in atherosclerosis. Circulation 2006;114:1504–1511. [PubMed: 17000904]
57. Kang HW, Josephson L, Petrovsky A, Weissleder R, Bogdanov A Jr. Magnetic resonance imaging of inducible e-selectin expression in human endothelial cell culture. Bioconjug Chem 2002;13:122–127. [PubMed: 11792187]
58. Reynolds PR, Larkman DJ, Haskard DO, Hajnal JV, Kennea NL, George AJ, Edwards AD. Detection of vascular expression of e-selectin in vivo with mr imaging. Radiology 2006;241:469–476. [PubMed: 17005768]
59. Funovics M, Montet X, Reynolds F, Weissleder R, Josephson L. Nanoparticles for the optical imaging of tumor e-selectin. Neoplasia 2005;7:904–911. [PubMed: 16242073]
60. Montet X, Weissleder R, Josephson L. Imaging pancreatic cancer with a peptide-nanoparticle conjugate targeted to normal pancreas. Bioconjug Chem 2006;17:905–911. [PubMed: 16848396]
61. Benedetto S, Pulito R, Crich SG, Tarone G, Aime S, Silengo L, Hamm J. Quantification of the expression level of integrin receptor alpha(v)beta3 in cell lines and MR imaging with antibody-coated iron oxide particles. Magn Reson Med 2006;56:711–716. [PubMed: 16958071]
62. Montet X, Montet-Abou K, Reynolds F, Weissleder R, Josephson L. Nanoparticle imaging of integrins on tumor cells. Neoplasia 2006;8:214–222. [PubMed: 16611415]
63. Moore A, Medarova Z, Potthast A, Dai G. In vivo targeting of underglycosylated muc-1 tumor antigen using a multimodal imaging probe. Cancer Res 2004;64:1821–1827. [PubMed: 14996745]

64. Schellenberger EA, Bogdanov A Jr, Hogemann D, Tait J, Weissleder R, Josephson L. Annexin v-clio: A nanoparticle for detecting apoptosis by MRI. Mol Imaging 2002;1:102–107. [PubMed: 12920851]

65. Schellenberger EA, Bogdanov A Jr, Petrovsky A, Ntziachristos V, Weissleder R, Josephson L. Optical imaging of apoptosis as a biomarker of tumor response to chemotherapy. Neoplasia 2003;5:187–192. [PubMed: 12869301]

66. Lewin M, Carlesso N, Tung CH, Tang XW, Cory D, Scadden DT, Weissleder R. Tat peptide-derivatized magnetic nanoparticles allow in vivo tracking and recovery of progenitor cells. Nat Biotechnol 2000;18:410–414. [PubMed: 10748521]

67. Wunderbaldinger P, Josephson L, Weissleder R. Tat peptide directs enhanced clearance and hepatic permeability of magnetic nanoparticles. Bioconjug Chem 2002;13:264–268. [PubMed: 11906263]

68. Weissleder R, Kelly K, Sun EY, Shtatland T, Josephson L. Cell-specific targeting of nanoparticles by multivalent attachment of small molecules. Nat Biotechnol 2005;23:1418–1423. [PubMed: 16244656]

69. Kelly KA, Setlur SR, Ross R, Anbazhagan R, Waterman P, Rubin MA, Weissleder R. Detection of early prostate cancer using a hepsin targeted imaging agent. Cancer Research. 2007In Press

70. Simberg D, Duza T, Park JH, Essler M, Pilch J, Zhang L, Derfus AM, Yang M, Hoffman RM, Bhatia S, Sailor MJ, Ruoslahti E. Biomimetic amplification of nanoparticle homing to tumors. Proc Natl Acad Sci U S A 2007;104:932–936. [PubMed: 17215365]

71. Reddy GR, Bhojani MS, McConville P, Moody J, Moffat BA, Hall DE, Kim G, Koo YE, Woolliscroft MJ, Sugai JV, Johnson TD, Philbert MA, Kopelman R, Rehemtulla A, Ross BD. Vascular targeted nanoparticles for imaging and treatment of brain tumors. Clin Cancer Res 2006;12:6677–6686. [PubMed: 17121886]

72. Funovics MA, Kapeller B, Hoeller C, Su HS, Kunstfeld R, Puig S, Macfelda K. Mr imaging of the her2/neu and 9.2.27 tumor antigens using immunospecific contrast agents. Magn Reson Imaging 2004;22:843–850. [PubMed: 15234453]

73. Sakamoto JH, Smith BR, Xie B, Rokhlin SI, Lee SC, Ferrari M. The molecular analysis of breast cancer utilizing targeted nanoparticle based ultrasound contrast agents. Technol Cancer Res Treat 2005;4:627–636. [PubMed: 16292882]

74. Wadghiri YZ, Sigurdsson EM, Sadowski M, Elliott JI, Li Y, Scholtzova H, Tang CY, Aguinaldo G, Pappolla M, Duff K, Wisniewski T, Turnbull DH. Detection of Alzheimer's amyloid in transgenic mice using magnetic resonance microimaging. Magn Reson Med 2003;50:293–302. [PubMed: 12876705]

75. Toma A, Otsuji E, Kuriu Y, Okamoto K, Ichikawa D, Hagiwara A, Ito H, Nishimura T, Yamagishi H. Monoclonal antibody a7-superparamagnetic iron oxide as contrast agent of mr imaging of rectal carcinoma. Br J Cancer 2005;93:131–136. [PubMed: 15970924]

76. DeNardo SJ, DeNardo GL, Miers LA, Natarajan A, Foreman AR, Gruettner C, Adamson GN, Ivkov R. Development of tumor targeting bioprobes ((111)Inchimeric l6 monoclonal antibody nanoparticles) for alternating magnetic field cancer therapy. Clin Cancer Res 2005;11:7087s–7092s. [PubMed: 16203807]

77. Kelly KA, Waterman P, Weissleder R. In vivo imaging of molecularly targeted phage. Neoplasia 2006;8:1011–1018. [PubMed: 17217618]

78. Hansson GK. Inflammation, atherosclerosis, and coronary artery disease. N Engl J Med 2005;352:1685–1695. [PubMed: 15843671]

79. Hansson GK, Libby P. The immune response in atherosclerosis: A double-edged sword. Nat Rev Immunol 2006;6:508–519. [PubMed: 16778830]

80. Libby P. Inflammation in atherosclerosis. Nature 2002;420:868–874. [PubMed: 12490960]

81. Trivedi RA, U-King-Im JM, Graves MJ, Cross JJ, Horsley J, Goddard MJ, Skepper JN, Quartey G, Warburton E, Joubert I, Wang L, Kirkpatrick PJ, Brown J, Gillard JH. In vivo detection of macrophages in human carotid atheroma: Temporal dependence of ultrasmall superparamagnetic particles of iron oxide-enhanced MRI. Stroke 2004;35:1631–1635. [PubMed: 15166394]

82. Jaffer FA, Nahrendorf M, Sosnovik D, Kelly KA, Aikawa E, Weissleder R. Cellular imaging of inflammation in atherosclerosis using magnetofluorescent nanomaterials. Mol Imaging 2006;5:85–92. [PubMed: 16954022]

83. Pande AN, Kohler RH, Aikawa E, Weissleder R, Jaffer FA. Detection of macrophage activity in atherosclerosis in vivo using multichannel, high-resolution laser scanning fluorescence microscopy. J Biomed Opt 2006;11021009

84. Nahrendorf M, Zhang H, Hembrador S, Panizzi PR, Sosnovik DE, Aikawa E, Libby P, Swirski FK, Weissleder R. Nanoparticle PET-CT imaging of macrophages in inflammatory atherosclerosis. Circulation. 2007In Press

85. McAteer MA, Sibson NR, von Zur Muhlen C, Schneider JE, Lowe AS, Warrick N, Channon KM, Anthony DC, Choudhury RP. In vivo magnetic resonance imaging of acute brain inflammation using microparticles of iron oxide. Nat Med 2007;13:1253–1258. [PubMed: 17891147]

86. Dhanasekaran SM, Barrette TR, Ghosh D, Shah R, Varambally S, Kurachi K, Pienta KJ, Rubin MA, Chinnaiyan AM. Delineation of prognostic biomarkers in prostate cancer. Nature 2001;412:822–826. [PubMed: 11518967]

87. McCarthy JR, Jaffer FA, Weissleder R. A macrophage-targeted theranostic nanoparticle for biomedical applications. Small 2006;2:983–987. [PubMed: 17193154]

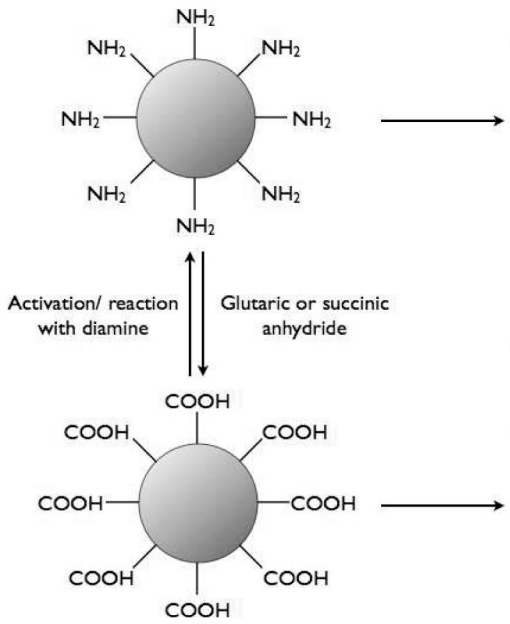

Action taken	Activating/reactive group	Molecules Conjugated
Activation towards sulfhydryl groups	SPDP SIA SMMC	Antibodies Peptides
Direct Reaction	Anhydrides Epoxides Succinimide esters Isothiocyanates	Small molecules Peptides Antibodies Dyes

Action taken	Activating/reactive group	Molecules Conjugated
Activation towards alcohols	Thionyl chloride	Small molecules
Activation/reaction	EDC/NHS or sulfo-NHS	Small, amine-containing molecules "Click" chemistry

Figure 1.
Bioconjugation of iron oxide nanoparticles.

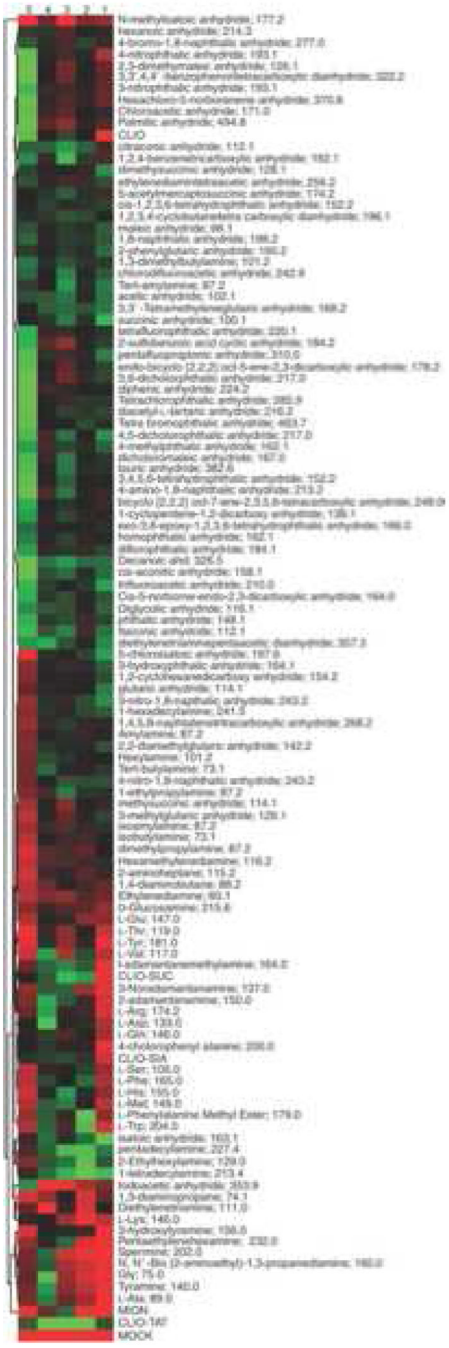

Figure 2.

Heat map representing cellular uptake of different nanoparticle preparations. Columns from right to left: 1, pancreatic cancer cells (PaCa-2); 2, macrophage cell line (U937); 3, resting primary human macrophages; 4, activated primary human macrophages; 5, human umbilical vein endothelial cells (HUVEC). Each column represents mean values from six different experiments. Red refers to the lowest accumulation and green refers to the highest accumulation [68].

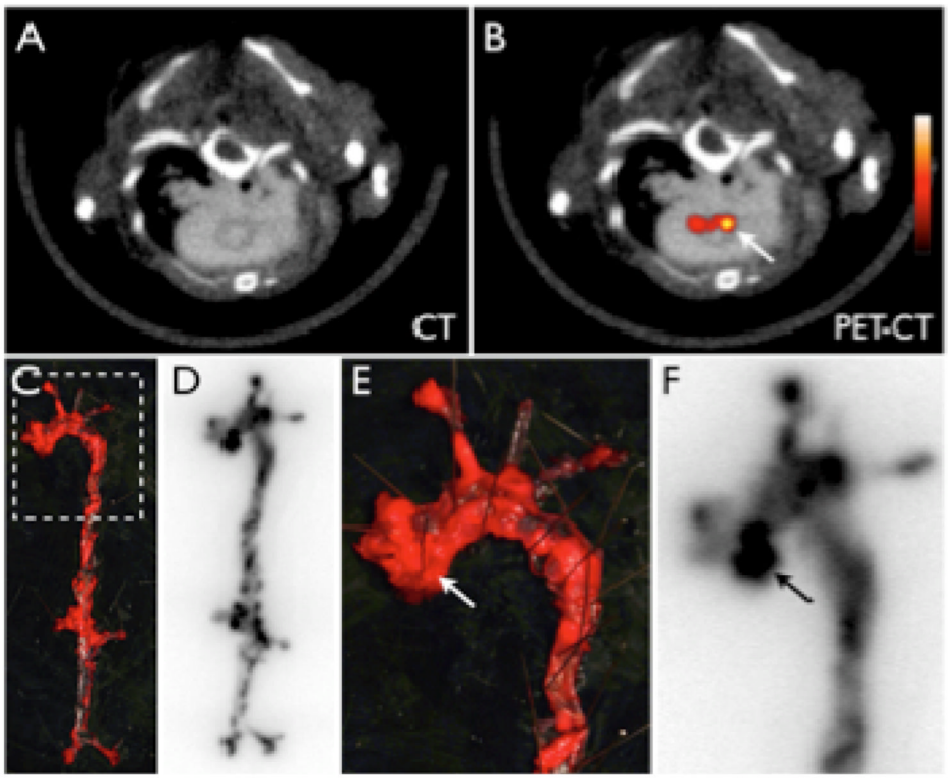

Figure 3.
^{64}Cu-CLIO distributes to atherosclerotic lesions. 5A–B: PET-CT shows enhancement of the posterior aortic root (arrow). 5C–F: En face Oil red O staining of the excised aorta depicts plaque loaded vessel segments, which co-localize with areas of high ^{64}Cu-TNP uptake on autoradiography. 5E–F show a zoomed image of the root and arch. The arrows depict a plaque laden segment of the root with high activity, which corresponds to the in vivo signal seen in 5B [84].

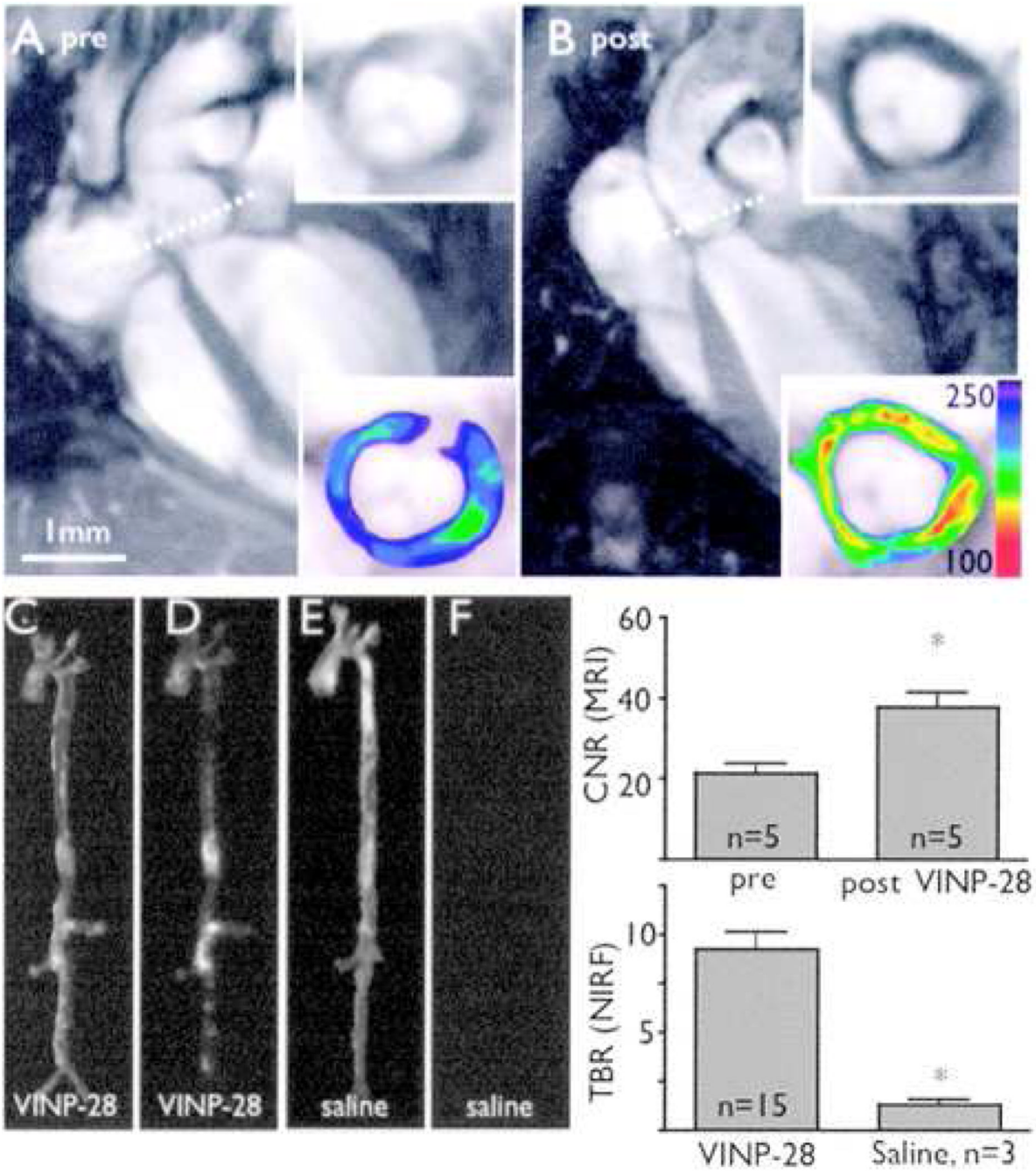

Figure 4.

In vivo MR and optical imaging of VCAM-1 expression. A, MRI before injection of targeted nanoagent. Dotted line depicts location of short-axis view (inserts, lower panel with color coded signal intensity). B, Same mouse 48 hours after injection. A marked signal drop in the aortic root wall was noted (insets). The contrast-to-noise ratio (CNR) of the aortic wall was increased significantly after injection of the probe (mean±SD; *P<0.05 before vs after injection). C, E, Light images of excised aortas. D, NIRF image after VINP-28 injection demonstrates distribution of the agent to plaque-bearing segments of the aorta, whereas the aorta of the saline injected apoE$^{-/-}$ shows very little fluorescent signal (F). Both images were acquired with

identical exposure times and were identically windowed. The target-to-background ratio (TBR) was significantly higher in the targeted nanoparticle injected mice (*P<0.05) [56].

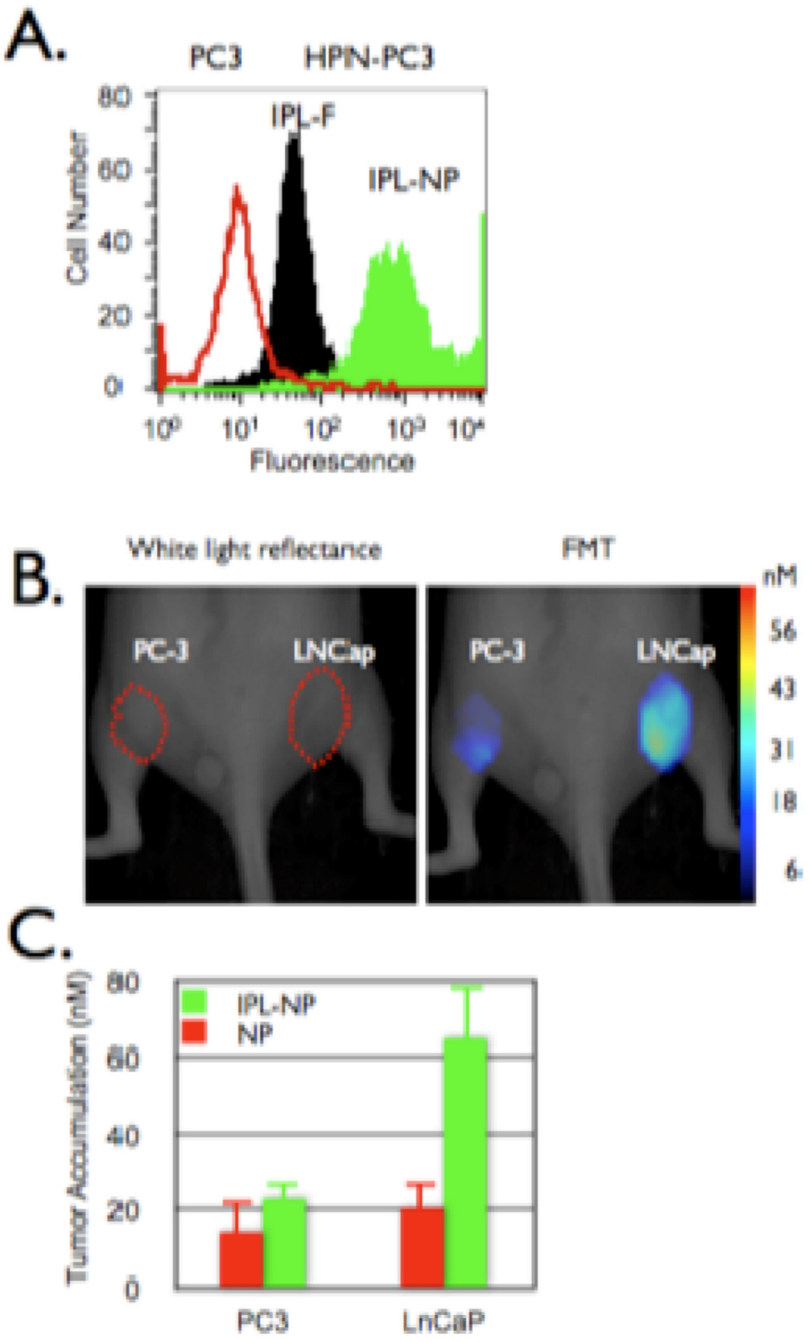

Figure 5.

In vivo imaging of prostate cancer. A. HPN-PC3 (black and green histograms) or PC3 (red histogram) cells were incubated with the HPN peptide or HPN peptide labeled nanoparticles (green histogram) then analyzed via flow cytometry. B and C. Mice bearing tumors derived from PC-3 (left flank) or LNCaP (right flank) were co-injected with HPN peptide labeled nanoparticles and a control nanoparticle (red bars) then (B) imaged and (C) accumulation quantified via FMT 24 hours post injection [69].

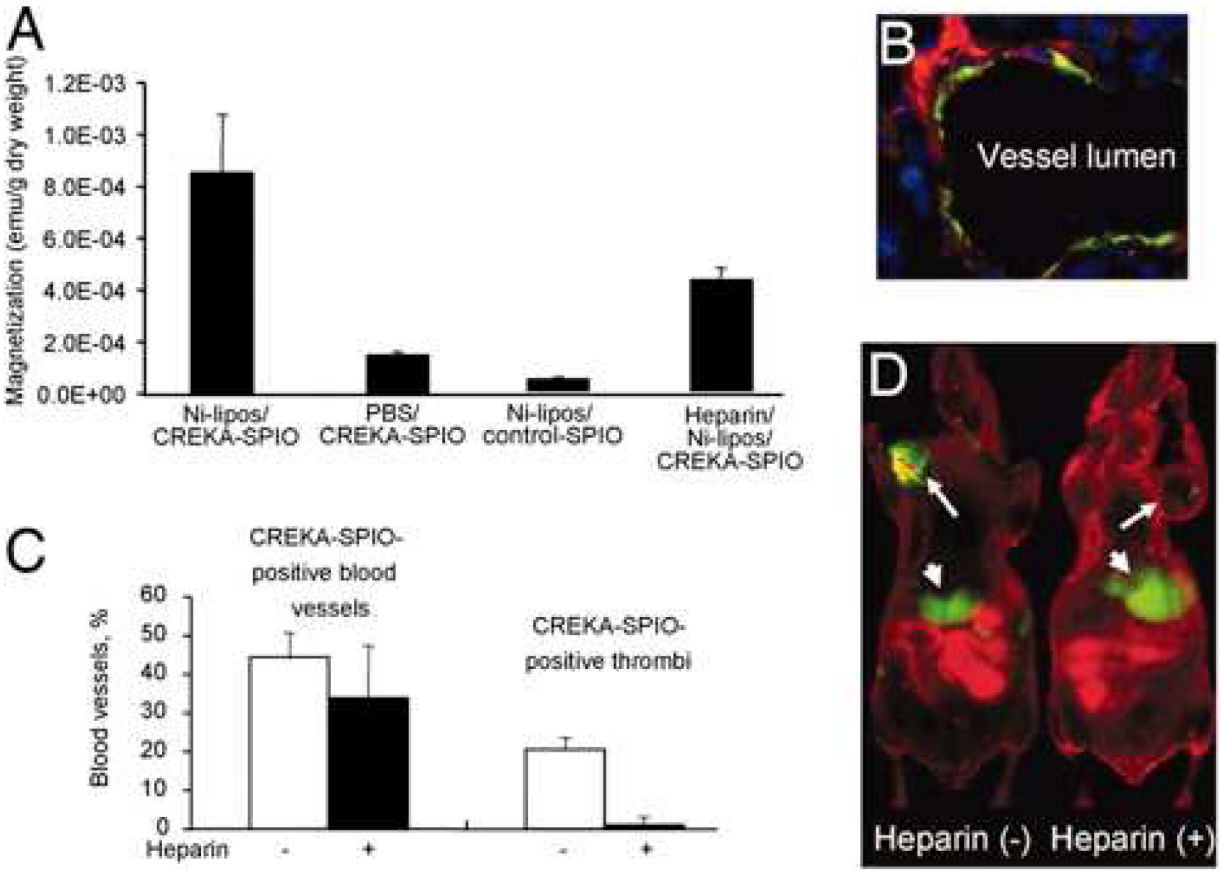

Figure 6.

Effect of blood clotting on nanoparticle accumulation in tumors. Mice bearing MDA-MB-435 human breast cancer xenografts were intravenously injected with PBS or heparin, followed by Ni-liposomes (or PBS) and CREKA-modified particles (or control nanoparticles). The mice received additional heparin by i.p. injections (a total of 1,000 units/kg) or PBS throughout the experiment. (A) Tumors were removed 6 h after the nanoparticle injection, and magnetic signal in the tumor after different treatments was determined with SQUID. (B) A representative example of the appearance of CREKA-targeted particles in tumor vessels of mice treated with heparin. (C) Quantification of heparin effect on clotting in blood vessels. Mice were pretreated with PBS (open bars) or heparin (filled bars) as described above, followed by Ni liposomes/ CREKA-targeted nanoparticles. Note that heparin did not significantly change the percentage of blood vessels containing particles, but dramatically decreased the incidence of the lumens that are filled with fluorescence. (D) Near-infrared imaging of mice that received Ni-liposomes, followed by Cy7-labeled CREKA-targeted particles, with or without heparin pretreatment. The images were acquired 8 h after the injection of the CREKA-targeted particles. Arrows point to the tumors, and arrowheads point to the liver [70].

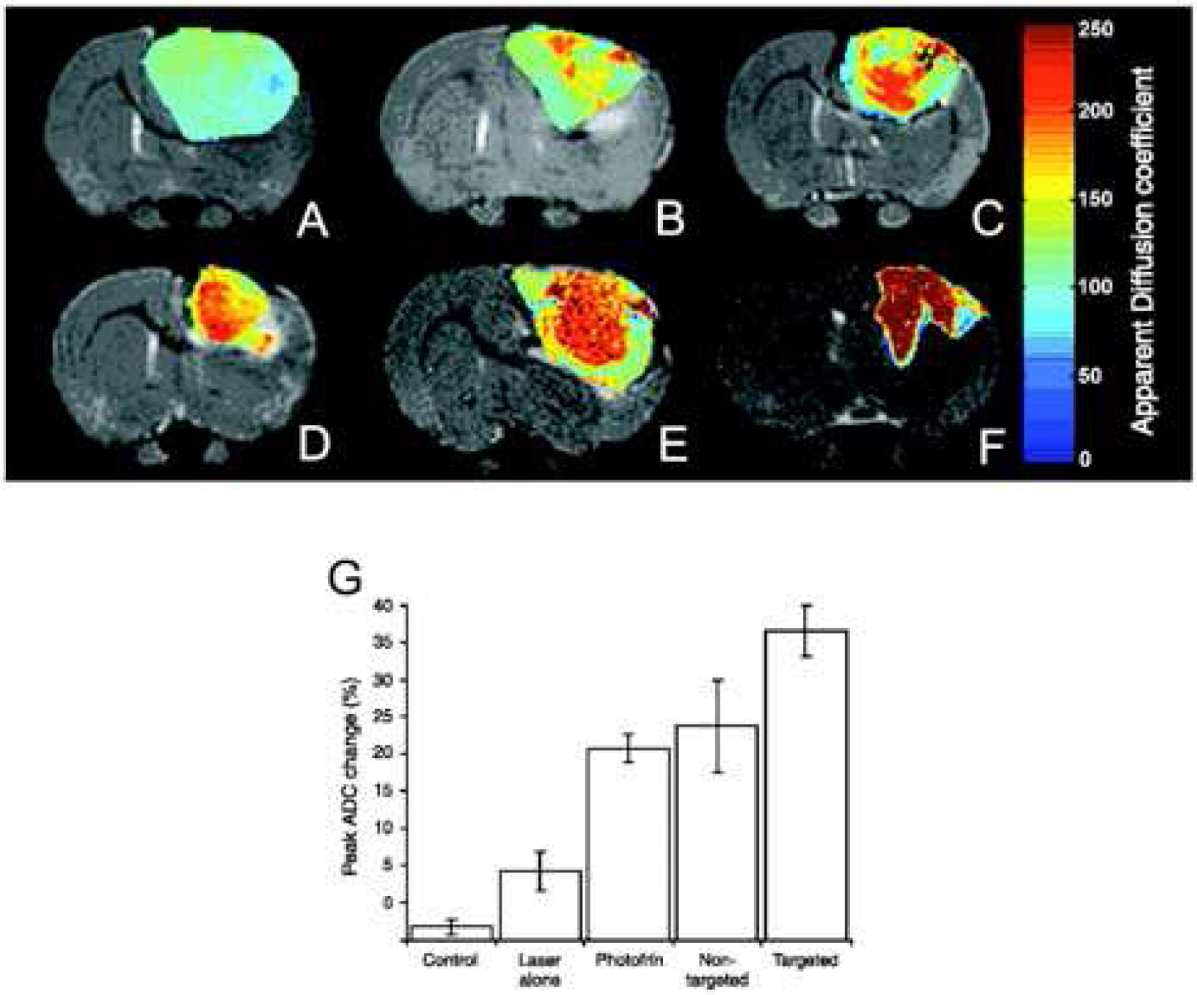

Figure 7.

Monitoring of therapeutic efficacy using multifunctional nanoparticles in 9L brain tumors. T2-weighted magnetic resonance images at day 8 after treatment from (C) a representative control i.c. 9L tumor and tumors treated with (D) laser light only, (E) i.v. administration of Photofrin plus laser light, and (F) nontargeted nanoparticles containing Photofrin plus laser light and (G) targeted nanoparticles containing Photofrin plus laser light. The image shown in (H) is from the same tumor shown in (G), which was treated with the F3-targeted nanoparticle preparation but at day 40 after treatment. The color diffusion maps overlaid on top of T2-weighted images represent the apparent diffusion coefficient (ADC) distribution in each tumor slice shown. I, columns, mean peak percentage change in tumor apparent diffusion coefficient values for each of the experimental groups; bars, SE [71].

Table 1

Targeted magnetic nanoparticle preparations utilized in vivo.

Target	Targeting Ligand	References
Engineered transferrin receptor	Holo-transferrin	[50–52]
	Anti-VCAM-1 antibody	[53]
VCAM-1	VHS peptide	[54]
	VINP peptide	[55,56]
	Anti-E-selectrin antibody	[57,58]
E-selectin	E-selectin binding peptide	[59]
Bombesin	Bombesin-like peptide	[60]
	Anti-αv antibody	[61]
αvβ3 integrin	RGD peptides	[46,62]
Muc-1	Muc-1 peptide	[63]
Phosphatidylserine	Annexin V	[64,65]
Cell label	Tat peptide	[16,66,67]
Macrophage subtypes	Small molecules	[68]
Hepsin	Hepsin peptide	[69]
Tumor vasculature	CREKA peptide	[70]
Tumor vasculature	F3 peptide	[71]
Her2/neu	Herceptin	[72,73]
Amyloid-β	Aβ 1–40 peptide	[74]
Colorectal carcinoma	Monoclonal antibody	[75]
Tumor associated antigen	Chimeric L6 antibody	[76]